SLAC-PUB-2745
May 1981
(T/E)

EXCLUSIVE FINAL STATES FROM PHOTON-PHOTON COLLISIONS AT SPEAR*

David L. Burke
Stanford Linear Accelerator Center
Stanford University, Stanford, California 94305

ABSTRACT

Studies of exclusive final states produced by the two-photon process have been made at SPEAR by the Mark II and by the Crystal Ball Collaborations. Measurements of $\pi^+\pi^-$ and $\pi^0\pi^0$ production in the mass region 500 MeV/c^2 < $m_{\pi\pi}$ < 2000 MeV/c^2 are presented. These data include strong signals from the well-known f(1270) meson. The A_2' has been observed via its $\pi^0\eta$ decay mode and its partial width to $\gamma\gamma$ has been determined. A measurement of the cross section for the reaction $\gamma\gamma \to \pi^+\pi^-\pi^+\pi^-$ is reported. This channel is found to be small just above the four pion threshold, but exhibits a large enhancement near the $\rho^0\rho^0$ threshold.

RESUMÉ

Une étude des états finaux exclusifs produits par le processus à deux photons a été faite à SPEAR par les collaborations travaillant avec MARK II et avec le Crystal Ball. Des mesures de la production de $\pi^+\pi^-$ et $\pi^0\pi^0$ dans la region de masse 500 MeV/c^2 < $m_{\pi\pi}$ < 2000 MeV/c^2 sont presentées ici. Ces données montrent un fort signal du bien connu meson f(1270). Le A_2(1310) a été aussi observé dans le mode de desintégration $\pi^0\eta$ et son amplitude partielle en $\gamma\gamma$ a été determinée. Une mesure de la section efficace de la reaction $\gamma\gamma \to \pi^+\pi^-\pi^+\pi^-$ est presentée. Ce canal est trouvé être faible juste au délà du seuil pour la production de 4π, mais montre un grand renforcement au voisinage du seuil de la production de $\rho^0\rho^0$.

I. INTRODUCTION

The production of a meson resonance or a meson-antimeson pair by two colliding photons is one of the simplest of hadronic reactions — strong interactions are present in only the final state. Photon-photon collisions are an ideal place to study the properties of $C = +$ resonances[1] ($J \neq 1$), and at higher masses the reaction $\gamma\gamma \to H\bar{H}$ is expected to be a testing ground for QCD.[2] Experimentally these processes can be readily identified by their unique kinematical properties. The $\gamma\gamma$ center-of-mass system is characterized by invariant masses that

* Work supported by the Department of Energy, contract DE-AC03-76SF00515.

(Invited Rapporteur presented at the 4th International Colloquium on Photon-Photon Interactions, Paris, France, April 6-9, 1981.)

are small compared to the e^+e^- center-of-mass energy, and by low transverse momenta relative to the beam axis. This latter property, which is due to the dominance of the incident flux by photons with small q^2, allows almost any topology to be isolated from feed-down from higher multiplicity events produced in the e^+e^- annihilation channel or in the two-photon channel itself.

Measurements of the cross section for the reaction $\gamma\gamma \to \pi^+\pi^-$ have been made with the Mark II detector at SPEAR, and the $\gamma\gamma \to \pi^0\pi^0$ process has been studied by the Crystal Ball group, also at SPEAR. Strong signals from the well-known f(1270) meson are seen in both final states, although the resonant mass appears to be $\approx 30-40$ MeV/c^2 below the value established in hadronic experiments. The large acceptance of the Crystal Ball detector allows, for the first time, a determination of the helicity structure of the production mechanism of the resonance. The cross section for the production of $\pi^+\pi^-$ pairs at masses above and below the resonant peak has been measured with the Mark II. The result is found to be quite large at masses below the resonance, but falls rather sharply at higher masses.

The $\pi^0\eta$ decay mode of the $A_2(1310)$ has been detected in the Crystal Ball. The measured decay width $\Gamma_{A_2 \to \gamma\gamma} \approx 0.8$ keV is in agreement with the value of 1.0 keV expected from SU(3) symmetry (with fractionally charged quarks) and the value $\Gamma_{f \to \gamma\gamma} \approx 2.7$ keV measured with the same detector.

The four pion final state, studied by the Mark II group, is found to be dominated by the process $\gamma\gamma \to \rho^0\rho^0 \to \pi^+\pi^-\pi^+\pi^-$. The cross section rises rapidly near the $\rho^0\rho^0$ threshold to a value ~100 nb. This is considerably larger than might be estimated from either the vector dominance model or from QCD.

The Crystal Ball detector[3] is shown in Fig. 1(a). It consists of two hemispheres made from geodesic arrays of sodium iodide crystals. When the endcap crystals are included, the detector is sensitive to electrons and photons that have laboratory polar angles that satisfy $|\cos\theta_L| < 0.98$. Proportional and drift chambers provide charge particle tracking, but there is no magnetic field. Although the detector is triggered by a variety of signals, two calorimetric triggers are most germane to the results given here. The Ball was triggered if each hemisphere recorded more than 150 MeV of deposited energy, or if

48

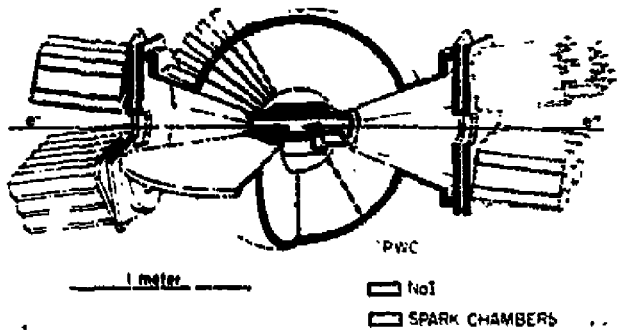

Fig. 1(a). The Crystal Ball Detector.

the sum of the deposited energy in the entire detector exceeded a pre-set threshold. This latter total-energy-threshold varied between 600 MeV and 1100 MeV for the data shown here.

The drift chamber and solenoid of the Mark II[4] (Fig. 1(b))

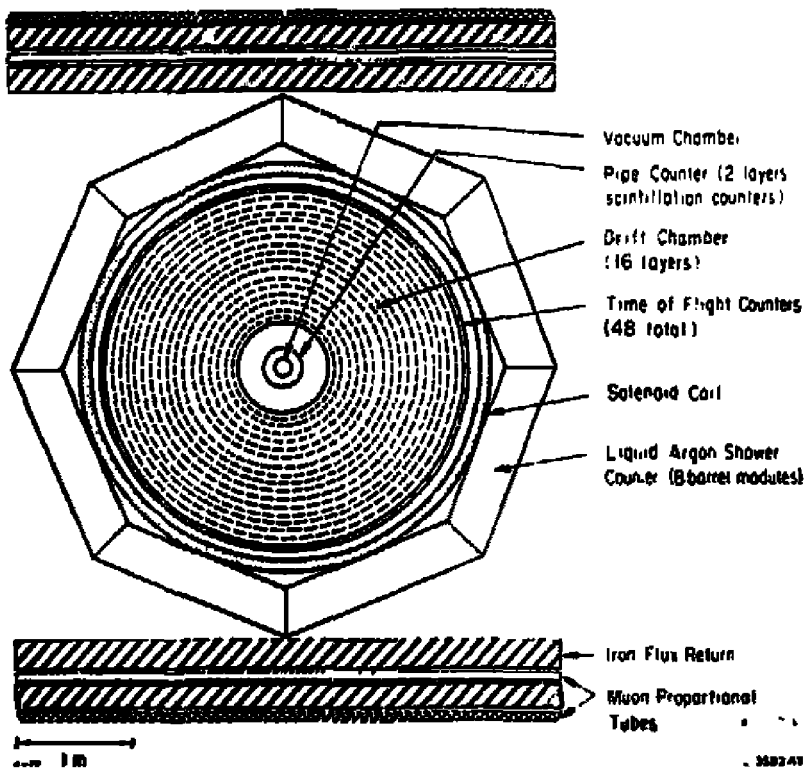

Fig. 1(b). The Mark II Detector.

comprise a charged particle spectrometer that covers the region defined by $|\cos\theta_L| \leq 0.8$. The acceptance of the liquid argon calorimeters that are located outside of the solenoid coil is approximately 65% of 4π. The detector was triggered by events with at least one charged track at $|\cos\theta_L| < 0.75$ and with $p_T \gtrsim 100$ MeV/c, and a second track at $|\cos\theta_L| \leq 0.85$.

II. $\gamma\gamma \to \pi^+\pi^-$

The two-prong mass spectrum, as seen in the Mark II, is given in Fig. 2. Events were selected if they contained two oppositely charged

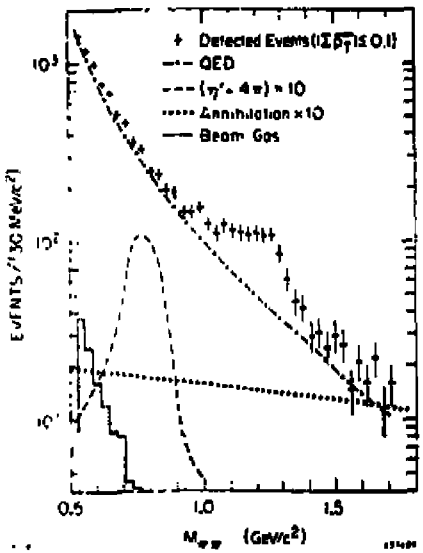

Fig. 2. Raw two-prong mass spectrum seen by the Mark II. The curves represent various contributions as measured and/or computed.

pronga, both with $|\cos\theta_L| < 0.6$, and no other charged particles. The net transverse momentum of the two tracks was required to be small, $|\Sigma \vec{p}_T| \leq 100$ MeV/c. The curves in Fig. 2 summarize the contributions to this sample made by various processes. Photon-photon production of the $\eta'(958)$ and $\rho^0\rho^0$ have been measured with the same detector (Ref. 4a and § VI below), so the feed-down from these sources has been

calculated with a Monte Carlo. The background from higher multiplicity events has been determined by making extrapolations from higher values of net transverse momentum. The beam-gas contamination was measured in side-bands of the vertex position along the beam axis. As can be seen, these backgrounds are quite small compared to the total two-prong sample, but they become 5 - 30% in the raw $\gamma\gamma \to \pi^+\pi^-$ signal discussed below.

Except in the region near 1200 MeV/c^2, the two-prong sample is dominated by QED events $\gamma\gamma \to ee$ and $\gamma\gamma \to \mu\mu$. The curve in Fig. 2 that represents these processes has been calculated with the Monte Carlo program of Smith and Vermaseren[5], and normalized by the measured luminosity of the experiment. Unfortunately this normalization is uncertain by ± 6%, hence a useful measurement of the $\gamma\gamma \to \pi^+\pi^-$ rate could not be made without increasing the $\pi\pi$/QED ratio. The necessary enhancement in the $\pi\pi$ signal over the QED background was achieved by making use of the relatively large probability that a low momentum pion will interact in the magnet coil before reaching the liquid argon; charge particles were identified as pions if they were within the fiducial area of the liquid argon, but deposited less energy in the liquid argon than would be expected from a minimum ionizing particle. The details of this identification procedure have been extensively studied with sources of pions, muons, and electrons that have been unambiguously identified without use of the liquid argon signals. At momenta $\geq$ 300 MeV/c, the pion identification probability is typically a factor of 10 larger than the muon and electron misidentification probabilities, although at momenta $\geq$ 500 MeV/c the pion acceptance is reduced to $\approx$ 15% per track.

The $\pi^+\pi^-$ signal was extracted from events which contained at least one identified pion and, separately, from events that were required to contain two identified pions. The results, given in Fig. 3(a), have been corrected for the QED background that remained in the raw data after the pion identification was made. The agreement between the results from the two levels of pion identification indicates that this remaining QED subtraction has been done reasonably well (the QED background in the 2π sample is completely negligible at mass $\gtrsim$ 700 MeV/c^2). The curve in the figure is the point-pion Born term[6] without any absorption corrections in the final state. Its normalization is absolute and it is included only as a theoretical reference

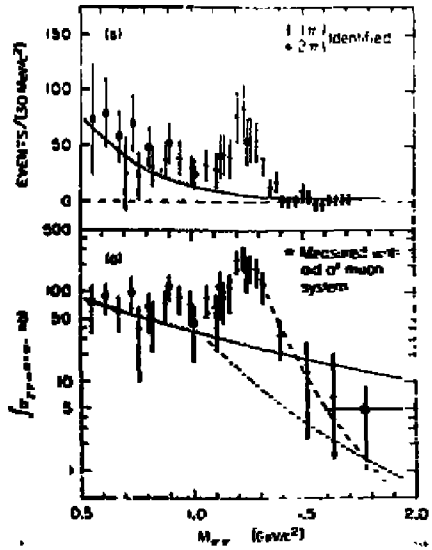

Fig. 3. (a) Fully corrected yield of $\pi^+\pi^-$ events with both prongs at $|\cos\theta_L| \leq 0.6$. No correction has been made for contamination by K^+K^- events; (b) The cross section $\sigma_{\gamma\gamma \to \pi^+\pi^-}$ integrated over the region $|\cos\theta^*| \leq 0.35$. — Born, and -·- QCD.

point. The number of pion pairs produced at masses below the resonance is seen to be quite large.

The results shown in Fig. 3(a) are not terribly convenient since they depend upon the detector acceptance and the spectrum of beam energies used in taking the data sample. The $\gamma\gamma$ cross section can be computed from[7]

$$\frac{d\sigma_{ee \to eeX}}{ds_X d\Omega^*} = \left(\frac{\alpha}{\pi}\right)^2 \frac{f(E_b, s_X)}{s_X} \frac{d\sigma_{\gamma\gamma \to X}(s_X)}{d\Omega^*} , \qquad (1)$$

where E_b is the beam energy, s_X is the square of the $\gamma\gamma$ invariant mass, and $d\Omega^*$ is the $\gamma\gamma$ c.m.s. solid angle element. With the restriction $|\cos\theta_L| < 0.6$, there is not much information in the angular distribution, but shown in Fig. 3(b) is the acceptance corrected cross section $\sigma_{\gamma\gamma \to \pi^+\pi^-}(m_{\pi\pi})$ integrated over the range $|\cos\theta^*| < 0.35$. Also included in this figure is a data point measured by using the

Mark II muon and liquid argon systems to directly reject electron and muon pairs. This point has been corrected for all backgrounds with previously described techniques. The data tend to fall below the point-pion Born cross section, and are consistent with the high mass tail of the f(1270) resonance. The prediction of a recent QCD calculation[2], also shown in the figure, indicates that data from PEP/PETRA will be needed in order to reach the interesting region at still higher masses.

It previously has been reported[8] that the resonance structure near 1200 MeV/c^2 is not consistent with the d-wave Breit-Wigner expected from parameters of the f(1270) determined in hadronic experiments. In particular the mass appears to be 30-40 MeV below the value 1273 ± 5 MeV/c^2 measured in $\pi^- p$ reactions. It can now be seen, however, that there is a significant amount of $\pi\pi$ production which is not accounted for by the resonant amplitude alone (Fig. 3). The data can be fitted by postulating that the non-f continuum interferes with the resonant Breit-Wigner in a manner similar to Söding model fits made to the ρ^0 mass distribution observed in photoproduction reactions $\gamma N \to \pi^+\pi^- N$[9]. The spectrum of Fig. 2 gives the best accuracy for such a study. The number of $\pi\pi$ events observed between 700 MeV/c^2 and 950 MeV/c^2 in Fig. 3(a) was used to normalize the QED curve in Fig. 2; the QED normalization was chosen such that the excess of events over QED in Fig. 2 is consistent with the number of $\pi\pi$ events observed in Fig. 3. The errors on the data of Figs. 2 and 3(a) result in a ± 4% uncertainty in the QED level. Shown in Fig. 4 is the spectrum that

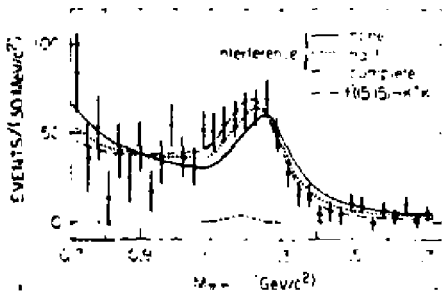

Fig. 4. The non-QED spectrum near the f(1270) mass. The K^+K^- component from the f'(1515) has been estimated by using SU(3) and BR(f' → K^+K^-) = 50%.

results from subtracting the QED distribution normalized by the central value of its allowed range. T is non-QED spectrum has been fitted by the sum

$$\pi\pi(m) = f(m) + \alpha \cdot C(m) + 2\beta \cdot \cos\delta(m) \cdot \sqrt{\alpha \cdot C(m) \cdot f(m)} + f'(m). \qquad (2)$$

In this equation, f(m) is the detected $\pi\pi$ yield appropriate for a relativistic d-wave Breit-Wigner with resonance mass and width equal to 1270 MeV/c^2 and 180 MeV/c^2, respectively. The resonance was assumed to be produced only with helicity ± 2, and all relevant photon flux factors have been included. Two extreme cases for the shape of the non-f $\pi\pi$ production, C(m), were considered. The first was the simple Born term at all masses, and the second consisted of using the Born term at masses below 1 GeV/c^2, but replacing it with the QCD prediction at higher masses (see Fig. 3(b)). The third term in Eq. (2) is a postulated interference between the first two terms. The non-f amplitude was taken to be real. Since no partial wave decomposition was done, the parameter β was included and fits were made with various values $-1 \leq \beta \leq 1$. The last term represents the contribution of the process $\gamma\gamma \to f'(1515) \to K^+K^-$ where the kaons have been misidentified as pions. The ratio $\Gamma_{f' \to \gamma\gamma} / \Gamma_{f \to \gamma\gamma}$ was taken from SU(3) and the $BR_{f' \to K^+K^-}$ was assumed to be 50%. The result of a Monte Carlo calculation, which included losses due to kaon decays, was that this term is 3.8% of the f. The yield of f' events is shown in Fig. 4 for the value of $\Gamma_{f \to \gamma\gamma}$ obtained below.

The fitted partial width of the f depends very little on either the QED normalization, the value of β, or the choice for the continuum. The result is (for helicity = ± 2)

$$\Gamma_{f \to \gamma\gamma} = 3.6 \pm 0.3 \text{ (statistical)} \pm 0.5 \text{ (systematic) keV}. \qquad (3)$$

Shown in Fig. 4 are the fits to the data that have been achieved for $\beta = 0$, 0.5, and 1.0 (with C(m) = Born). If the non-f continuum is parametrized by the QCD prediction above $m_{\pi\pi} = 1.0$ GeV/c^2 then the fitted values of $\Gamma_{f \to \gamma\gamma}$ increase by ≈ 10% (included in the systematic error), and the data prefer a somewhat larger value of β.

III. $\gamma\gamma \to \pi^0\pi^0$

The absence of a QED background to the $\pi^0\pi^0$ final state makes this a particularly clean hadronic channel. Furthermore, the direct coupling of photons to neutral pions is expected to be small, so resonance structure, such as the f, can be studied in a relatively straightforward manner. The Crystal Ball detector is beautifully matched to this process. Events were selected as $\pi^0\pi^0$ candidates if they contained four photons with total visible energy in excess of 700 MeV and no charged tracks. The distribution of the square of the net transverse momentum, $|\Sigma \vec{p}_T|^2$, of all such events is shown in Fig. 5(a). The distribution of the invariant mass of the photons in events with $|\Sigma \vec{p}_T|^2 \leq 0.03$ GeV$^2/c^2$ is shown in Fig. 5(b).

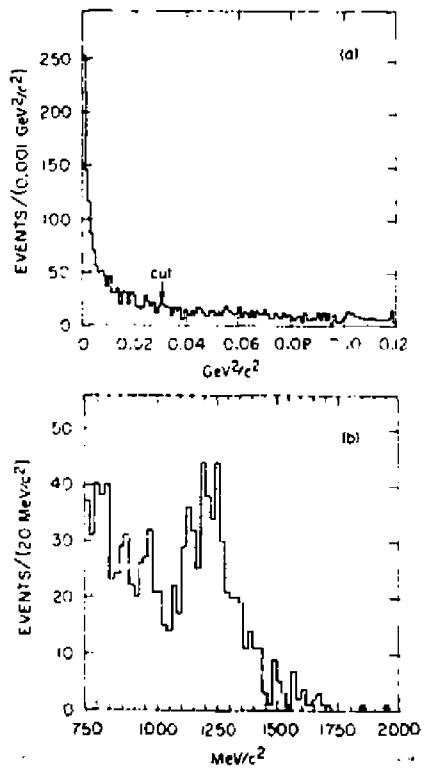

Fig. 5. (a) The $|\Sigma \vec{p}_T|^2$ distribution for 4γ events as seen by the Crystal Ball. (b) Invariant mass, $m_{4\gamma}$, for events with $|\Sigma \vec{p}_T|^2 \leq 0.03$ GeV$^2/c^2$.

For demonstration purposes, events were selected with $1040\ \text{MeV}/c^2 \leq m_{4\gamma} \leq 1480\ \text{MeV}/c^2$ (i.e., the f(1270) mass range) and the scatter plot of photon pair masses (three combinations per event) shown in Fig. 6 was constructed. In addition to the spectacular $\pi^0\pi^0$ signal, a cluster of $\pi^0\eta$ events is clearly discernable.

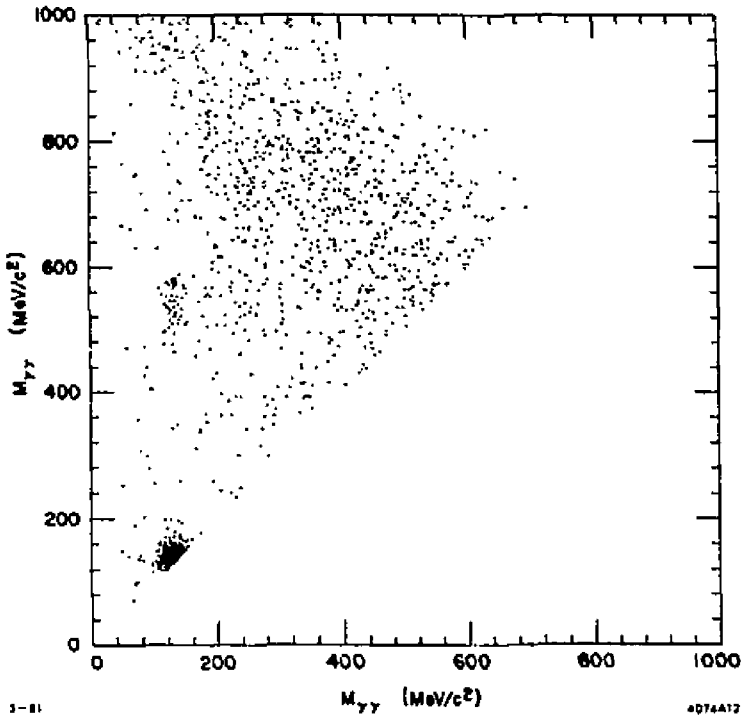

Fig. 6. Scatter plot $m_{\gamma\gamma}$ against $m_{\gamma\gamma}$ for events with $m_{4\gamma}$ in the f(1270) region. There are three entries per event.

The $\gamma\gamma \to \pi^0\pi^0$ signal has been extracted from the total sample of 4γ events (with $|\Sigma \vec{p}_T|^2 \leq 0.03\ \text{GeV}^2/c^2$) by making a two-dimensional cut that required a $\pi^0\pi^0$ combination to exist with $100\ \text{MeV}/c^2 \leq m_{\gamma\gamma} \leq 170\ \text{MeV}/c^2$. Backgrounds from other processes were measured in two-dimensional sidebands around the $\pi^0\pi^0$ area. They were found to be quite small at invariant masses above 800 MeV/c^2. Beam-gas backgrounds were estimated to be $\lesssim 1\%$. The background-subtracted $\pi^0\pi^0$ mass plot is given in Fig. 7(a). The subset of these data that was taken with a low total-energy-trigger threshold (600 MeV to

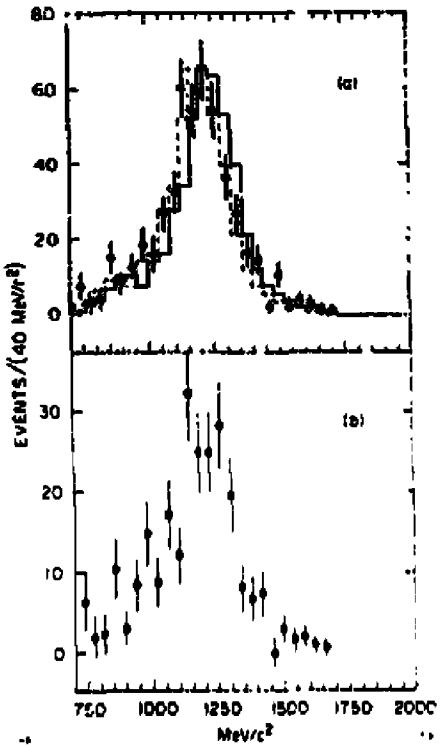

Fig. 7. Background-subtracted $\pi^0\pi^0$ mass spectrum. (a) All events, and (b) the subset taken with a low trigger threshold. The solid histogram is a Monte Carlo described in the text, and the dashed histogram is the solid histogram shifted downward one bin (40 MeV).

800 MeV) is shown in Fig. 7(b). Although there may be a slightly larger portion of events below 1000 MeV/c^2 in the low-threshold data, it appears that the remainder of the trigger scheme was sufficient to prevent any serious distortion of the mass spectrum.

The data in Fig. 7 have neither been corrected for detection efficiency nor has the distortion due to the photon flux been removed.

The solid histogram in the figure is a Monte Carlo simulation of the distribution (approximately normalized to the data) that is expected to be produced by the f(1270) assuming the nominal mass and width. Relevant efficiencies (except the trigger) and photon flux factors have been included in the Monte Carlo. The detector efficiency falls smoothly from ≈ 35% at 800 MeV/c^2 to ≈ 15% at 1600 MeV/c^2. The dotted line, which is the same histogram shifted downward by one bin (40 MeV/c^2) gives a good description of the complete spectrum at masses ≥ 700 MeV/c^2.

As a check on the calibration of the energy scale of the crystals in the detector, the π^0 mass spectrum from events in the f region (1040 MeV/c^2 - 1480 MeV/c^2) was examined. The π^0 mass was found to be 134.8 ± 0.6 MeV/c^2 which can be compared with the value 135.8 ± 0.3 MeV/c^2 predicted by the Monte Carlo. The energy scale was deliberately altered by 3% (the amount needed to account for the shift in the f mass) and the analysis of the data was repeated. The π^0 mass was then found to be 138.5 ± 0.6 MeV/c^2. It would appear that if the shift in the f mass is created by the detector, then it is not a simple linear error in the energy calibration. It must be noted that the mass of the η(549) as measured by the Ball has at times been as much as 1.5 - 2.0% below its accepted value.

The large acceptance of the Crystal Ball makes it possible to study the angular distribution of the $f \to \pi^0\pi^0$ decay. Most theoretical models[1] expect the production of the f to be dominated by photon pairs that have opposite helicity ($\lambda = 2$). The observed distribution of the angle in the γγ c.m.s. between one of the outgoing π^0's and the incoming e^- is given in Fig. 8 (The incident photons are primarily at angles ~ m_e/E_b with respect to the beam axis). This distribution has been fitted by the form

$$\frac{d\sigma}{d(|\cos\theta^*|)} = a_0|Y_2^0|^2 + a_1|Y_2^1|^2 + a_2|Y_2^2|^2 \quad , \qquad (4)$$

which is valid since the experimental data have been integrated over the azimuthal angle. The result of this fit is included in Fig. 8 and, as can be seen, the $\lambda = 2$ piece is dominant; $a_0/a_2 = 0.12 \pm 0.39$ and $a_1/a_2 = 0.02 \pm 0.11$. Alternatively, a fit of the distribution to a sum of the f with $\lambda = 2$ and an s-wave background yields the ratio

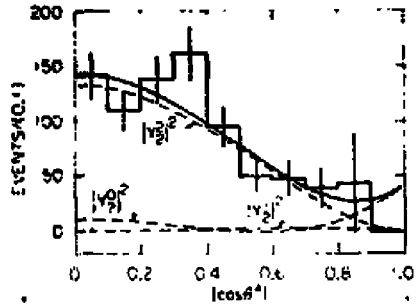

Fig. 8. Decay angular distribution in the process $f(1270) \to \pi^0\pi^0$. The curves are a fit described in the text.

$a_{s\text{-wave}}/a_2 = 0.05 \pm 0.25$.

Knowledge of the helicity structure of the $\gamma\gamma \to f$ production mechanism is also important because the experimental acceptance of most detectors depends critically on the f decay distribution. After computing the acceptance of the Crystal Ball for each helicity channel and weighting the overall acceptance by the measured helicity fractions, the partial width of the f to $\gamma\gamma$ was found to be

$$\Gamma_{f \to \gamma\gamma} = 2.90 \,^{+.55}_{-.39} \text{ (statistical)} \pm 0.58 \text{ (systematic) keV.} \qquad (5)$$

This is the only measurement of $\Gamma_{f \to \gamma\gamma}$ made to date that does not rely on an assumed helicity structure of the production mechanism. In order to allow comparisons with other results, a value of $\Gamma_{f \to \gamma\gamma} = 2.7 \pm 0.2 \pm 0.6$ keV has been computed from the observed number of events under the assumption that the f is produced only in the helicity ±2 state (this is the assumption usually made by other experimenters, e.g., result (3) above).

IV. The f(1270) at SPEAR

The two measurements of the radiative width of the f presented here, 2.7 ± 0.2 ± 0.6 keV (Crystal Ball) and 3.6 ± 0.3 ± 0.5 keV (Mark II), can be compared with the value 2.3 ± 0.5 ± 0.35 previously published by the PLUTO collaboration[10,11]. (These values all assume helicity ± 2.) A variety of theoretical approaches have led to pre-

dictions for the absolute size of $\Gamma_{f \to \gamma\gamma}$ that lie between ≈ 4 keV and 20 keV[1]. The experimental values are consistently a factor of 2 to 7 smaller than these expectations, and place constraints on the models which, in some cases, may be fatal.

The mass of the f produced in γγ collisions appears to be 30 – 40 MeV/c^2 below the value established by phase-shift analyses of hadronic reactions[12]. This shift of ≈ 3% has been reproduced in the charged final state by postulating the existence of an interference with the measured non-f $\pi^+\pi^-$ production. The apparent absence of a non-f component in the $\pi^0\pi^0$ final state, however, eliminates this mechanism in the neutral channel. The possibility that the observed $\pi^0\pi^0$ shift arises from a geometrical problem in the Crystal Ball detector is still being pursued[13].

It is, of course, well known that broad resonances produced in photoproduction experiments (e.g., $\gamma N \to \rho^0 N$) are observed to have distorted line shapes[2]. These effects, however, are confined primarily to the diffractive kinematic region at low momentum transfers, and have been thought to be due to interference with other amplitudes[14] or to properties peculiar to the corresponding hadronic diffractive process predicted by VMD[15] (e.g., $\rho^0 N \to \rho^0 N$). If the data presented in this report are taken at face value, then neither of these ideas is sufficient by itself to explain the process $\gamma\gamma \to f \to \pi\pi$.

V. $\gamma\gamma \to \pi^0\eta$

The $\pi^0\eta$ signal seen in Fig. 6 has been analyzed in the same manner as the $\pi^0\pi^0$ signal. After making sideband background subtractions, the mass plot shown in Fig. 9 is obtained. A signal of 25 events over a background of 5 – 6 events is seen at the mass of the A_2(1310). There are not enough events to allow determination of the decay distribution, but with the resonance assumed to be produced with helicity ± 2 the partial width has been computed to be

$$\Gamma_{A_2^0 \to \gamma\gamma} = 0.77 \pm 0.18 \text{ (statistical)} \pm 0.27 \text{ (systematic) keV.} \quad (6)$$

The A_2^0(1310) and the f(1270) are thought to be nearly degenerate $I_z = 0$ members of an ideally mixed 2^{++} nonet. Nonet symmetry predicts

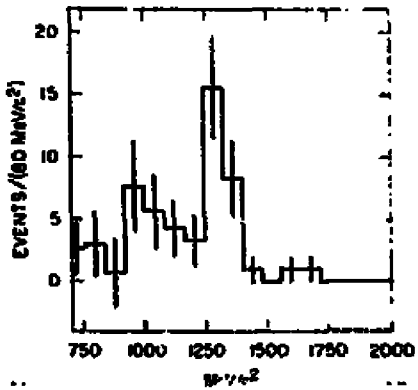

Fig. 9. Background-subtracted $\pi^0\eta$ mass spectrum seen by the Crystal Ball. Data with $|\Sigma \vec{p}_T|^2 \leq 0.03$ GeV^2/c^2.

the ratio $\Gamma_{f \to \gamma\gamma} / \Gamma_{A_2^0 \to \gamma\gamma} \cdot 25/9$ if quarks are fractionally charged. The Crystal Ball measurements give the experimental result $2.7/.77 \approx 27/8$. It should be pointed out that even though a number of systematic uncertainties might cancel in the ratio, the statistical errors are still large. Nevertheless, the agreement with the SU(3) prediction is notable.

VI. $\gamma\gamma \to \pi^+\pi^-\pi^+\pi^-$

The four pion final state has been studied with the Mark II using all data taken with beam center-of-mass energies between 4.8 GeV and 6.5 GeV (≈ 12 pb^{-1}). The mass spectrum of all events that contain four charged tracks with zero total charge is given in Fig. 10 for two different cuts on the net transverse momentum of the particles. In addition to exclusive signals at the beam center-of-mass energies (approximately half of the data were acquired at $\sqrt{s} \approx 5.2$ GeV), there is a clear structure around 1.5 GeV/c^2. The detector trigger threshold was ≈ 700 MeV/c^2 and turned on rather sharply. Only events with invariant masses below 3.0 GeV/c^2 were further considered.

Backgrounds from beam-gas events were found to be only a few percent and corrections have been made to all data shown here. Feed-down from higher multiplicity events produced in either the annihilation channel or the two-photon channel itself were subtracted by making

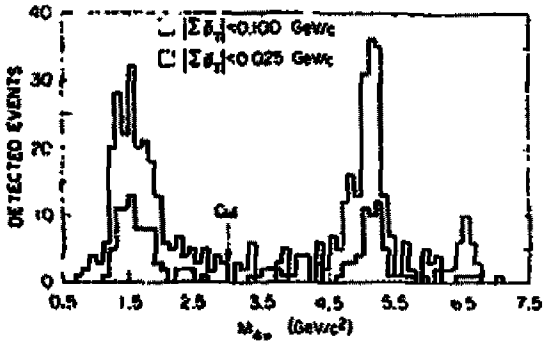

Fig. 10. Raw four-prong mass spectrum seen by the Mark II. Data with two different cuts on the transverse momentum $|\Sigma \vec{p}_T|$ are shown.

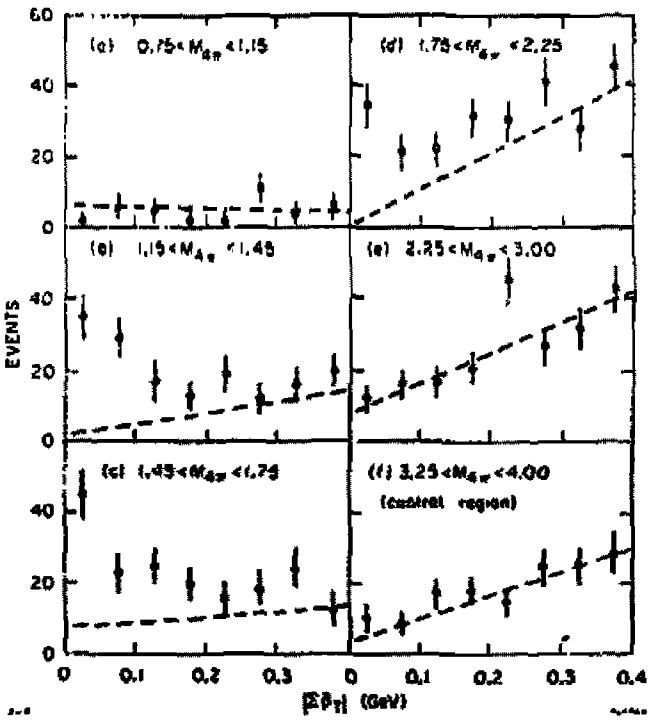

Fig. 11. Distributions in the $|\Sigma \vec{p}_T|$ variable. The lines are estimates of the background to the two-photon signal.

extrapolations in the net transverse momentum variable. Shown in Fig. 11 are the p_T distributions in each of several mass bins. The dashed lines are estimates of the feed-down backgrounds that have been made by fitting these distributions with the known shape of the two-photon process and an assumed straight line shape for the background. The numbers of two-photon events with total transverse momentum less than 100 MeV/c as determined by the fits were taken to be the signal. The errors on these numbers were also determined by the fits and, thus, include a reasonable estimate of the systematic uncertainty of the background subtraction. (This uncertainty dominates the errors in the final answers given below.)

Before the acceptance of the detector for the process $\gamma\gamma \to 4\pi$ was determined, the phase space structure that the data exhibit was studied. Each event contains 4 neutral combinations of $\pi^{\pm}\pi^{\mp}$ and 2 charge-two combinations $\pi^{\pm}\pi^{\pm}$. If the pions are pair-wise uncorrelated, then the mass distribution of $\pi^{\pm}\pi^{\mp}$ pairs would have the same shape as that for $\pi^{\pm}\pi^{\pm}$. The relative normalization, furthermore, would just be a factor of 2. The mass distribution of charge-zero pairs is shown in Fig. 12(a) as points with errors, and the same distribution for charge-two pairs is given as a histogram. The shapes are quite different; the neutral pairs are peaked near the ρ mass. If the pions are completely correlated as $\rho^0\rho^0$, then the mass distribution of pairs formed by a π^+ from a ρ^0 and a π^- from the other ρ^0 is approximately equivalent to the charge-two distribution. The equivalence here is only approximate because Bose symmetry, applied to the four pion final state, introduces structure into the like-sign mass spectrum. Figure 12(b) shows the result of subtracting the $\pi^{\pm}\pi^{\pm}$ spectrum from the $\pi^{\pm}\pi^{\mp}$ spectrum. The histogram in this figure is the result of a Monte Carlo calculation using a mass matrix which is the square of the symmetrized coherent sum of two relativistic p-wave Breit-Wigner amplitudes. Events were generated separately in each mass bin, renormalized to the number of events observed in each bin, and finally added together. The same subtraction of the charge-two distribution from the neutral pair distribution was then done. Scatter plots of the mass of one pair opposite the remaining pair are shown in Fig. 13 for the mass bins that contain a measurable signal. Maximum likelihood fits to these plots have been done using a combination of the

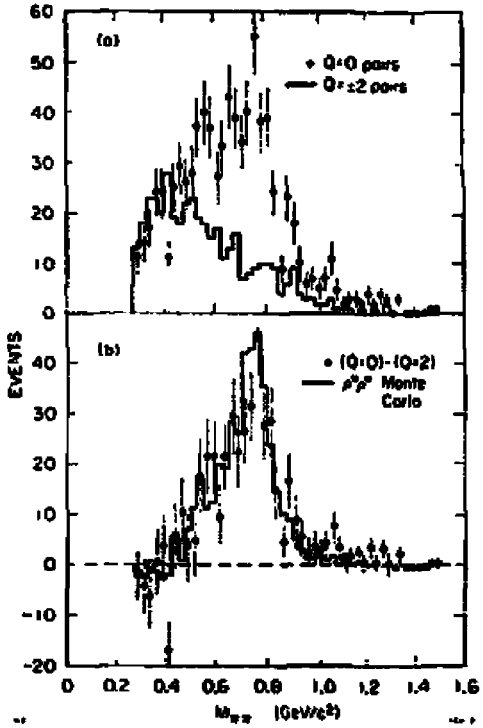

Fig. 12. Two-pion mass distributions. (a) Masses for like-sign and opposite-sign pairs, and (b) the difference between opposite-sign and like-sign distributions. The histogram in (b) is a Monte Carlo described in the text.

$\rho^0\rho^0$ matrix element and pure phase space. The fits are consistent with the two-photon signal being all $\gamma\gamma \to \rho^0\rho^0$, but cannot rule out a $\gamma\gamma \to 4\pi$ (phase space) component as large as 15–20% in any given mass bin.

The production and decay angular distributions of the ρ^0's provide additional information about the production mechanism(s) occurring in this mass region. The subtraction technique used to produce Fig. 12(b) gives the efficiency corrected distribution of the ρ^0 production angle (in the $\gamma\gamma$ c.m.s.) shown in Fig. 14(a). The corresponding distribution of the ρ^0 decay angle (in the ρ^0 rest frame) is given in Fig. 14(b). Although the errors are large (and the points are correlated to each other), the ρ^0 production appears to be peaked

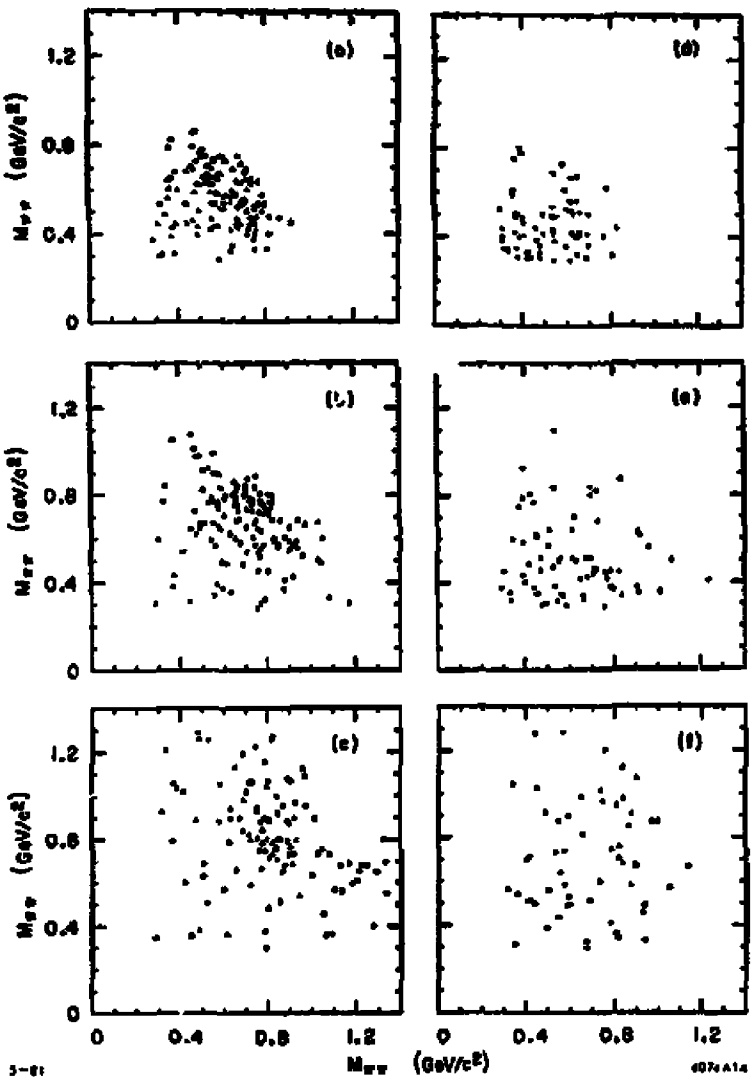

Fig. 13. Goldhaber plots. (a), (b), and (c) are opposite-sign pairs in the mass ranges
(a) 1.15 GeV/c^2 < $M_{4\pi}$ < 1.45 GeV/c^2,
(b) 1.45 GeV/c^2 < $M_{4\pi}$ < 1.75 GeV/c^2, and
(c) 1.75 GeV/c^2 < $M_{4\pi}$ < 2.25 GeV/c^2.
The plots (d), (e), and (f) are for the corresponding like-sign pairs.

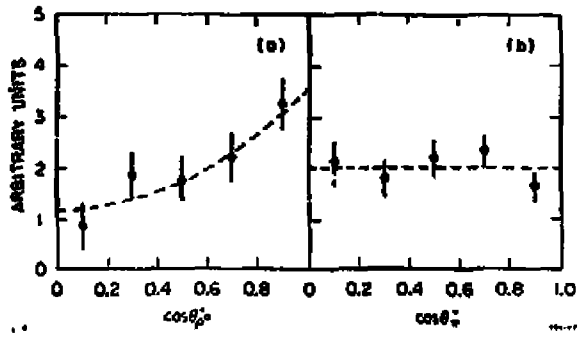

Fig. 14. (a) Production and (b) decay distributions for ρ^0. Events with total mass between 1.15 GeV/c^2 and 2.25 GeV/c^2. A curve of the form $a+b\cos^2\theta^*_\rho$ is shown in (a).

fore and aft. The decay distribution is quite flat, which would indicate that the ρ^0's are not produced with the helicity of the incident photons.

The acceptance of the detector was calculated with the Monte Carlo by using the $\rho^0\rho^0$ matrix element for the $\pi^+\pi^-$ mass weighting, and using angular distributions consistant with Fig. 14. The cross section $\sigma_{\gamma\gamma \to 4\pi}$ was the calculated (Eq. (2) integrated over $d\Omega^*$), and the results are displayed in Fig. 15. After the background subtraction, no signal was left in either the highest or in the lowest mass bins, so one standard deviation limits are given. Shown also in the figure are the results for $\gamma\gamma \to \rho^0\rho^0$ that have been previously reported by the TASSO collaboration[16]; the two results are in reasonable agreement.

A current algebra calculation[17] of the process $\gamma\gamma \to \pi^+\pi^-\pi^+\pi^-$ has given a value ~ 2nb for the cross section just above the four-pion threshold. A perturbative QCD calculation of the cross section $\gamma\gamma \to \rho^0\rho^0$ has recently been completed[2] and, although its validity at low masses is uncertain, the result is given in Fig. 15 as a theoretical reference point. Alternatively, vector dominance suggests the estimate

$$\sigma_{\gamma\gamma \to \omega\rho} \sim \left(\frac{1}{250}\right)^2 \sigma_{\rho\rho \to \rho\rho} \sim \left(\frac{1}{250}\right)^2 \left(\frac{\sigma^{el}_{np}}{\sigma^{el}_{pp}}\right)^2 \sigma^{el}_{pp} \sim 30 \text{ nb} \qquad (7)$$

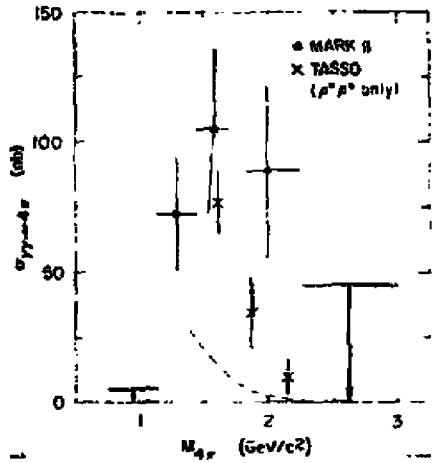

Fig. 15. Measured cross sections for $\gamma\gamma \to \pi^+\pi^-\pi^+\pi^-$. Errors assigned to the Mark II data include all known systematic contributions. The TASSO data are for $\gamma\gamma \to \rho^0\rho^0$ only. The curve is a theoretical prediction described in the text.

for the cross section, again at large c.m.s. energies. The observed cross section near the $\rho^0\rho^0$ threshold is considerably larger than these values. Recently, Laysac and Renard have interpreted this enhancement as evidence for a 0^{-+} glueball with mass ≈ 1600 MeV/c^2 [18]. Goldberg and Weiler have argued that the data are consistent with a 2^{-+} orbital excitation of the $\eta(549)$ [19]. Both of these assumptions are able to fit the observed mass dependence of the cross section, but the angular distribution of the ρ^0's (Fig. 14(a)) would favor a spin-2 object.

ACKNOWLEDGEMENT

The beautiful results on the $\pi^0\pi^0$ and $\pi^0\eta$ final states that are presented here are primarily the work of K. Wacker of the Crystal Ball Collaboration. The author wishes to thank him for providing these preliminary and unpublished data and for invaluable discussions. I also wish to thank Prof. G. London, his staff, and the University of Paris for a most exciting and informative conference.

REFERENCES

1. F. J. Gilman, SLAC-PUB-2461, 1980. Presented at the Internat. Conf. on Two-Photon Interactions, Lake Tahoe, Calif. 1979. M. Greco, LNF-80/28 (p), 1980. Presented at the Internat. Workshop on $\gamma\gamma$ Collisions, Amiens, France, 1980.
2. S. J. Brodsky and G. P. Lepage, SLAC-PUB-2587, 1980. See also, G. P. Lepage, Rapporteur presentation to this conference.
3. E. D. Bloom, invited talk XIV Rencontre de Morion, 1979; G. Godfrey, IEEE Trans. on Nucl. Sci. NS-25, no. 1, 333 (1978).
4. G. S. Abrams et al., Phys. Rev. Lett. 43, 477 (1979); R. H. Schindler, SLAC Report-219, Ph.D. Thesis (1979), unpublished.
5. J. Smith, J. A. M. Vermaseren, and G. Grammer, Phys. Rev. D15, 3220 (1977).
6. S. J. Brodsky, T. Kinoshita, and H. Terazawa, Phys. Rev. D4, 1532 (1971).
7. G. Bonneau, M. Gourdin, and F. Martin, Nucl. Phys. B54, 573 (1973); J. H. Field, Nucl. Phys. B168, 477 (1980).
8. A. Roussarie, SLAC-PUB-2599. Presented at the 20th Internat. Conf. on High Energy Physics, Madison, Wisc., 1980.
9. J. Ballam et al., Phys. Rev. D5, 545 (1972); G. E. Gladding et al., Phys. Rev. D8, 3721 (1973).
10. PLUTO Collab., Ch. Berger et al., Phys. Lett. 94B, 254 (1980).
11. A value for $\Gamma_{\xi \to \gamma\gamma}$ has also been given by the TASSO collaboration. See E. Hilger, Rapporteur presentation to this conference.
12. For a review see, W. Männer, Proc. Conf. on Experimental Meson Spectroscopy, Boston, 1974.
13. K. Wacker, Crystal Ball Collab., private communication.
14. P. Söding, Phys. Lett. 19, 702, 1965.
15. M. Ross and L. Stodolsky, Phys. Rev. 149, 1172 (1966).
16. TASSO Collab., R. Brandelik et al., Phys. Lett. 97B, 448 (1980).
17. H. Terazawa, Phys. Rev. Lett. 26, 1201 (1971).
18. J. Layssac and F. M. Renard, PM/80/11, 1980.
19. H. Goldberg and T. Weiler, NUB # 2488, 1981.